Size effects on negative thermal expansion in cubic ScF_3

C. Yang, P. Tong', J. C. Lin, X. G. Guo, K. Zhang, M. Wang, Y. Wu, S. Lin, P. C. Huang, W. Xu, W. H. Song, and Y. P. Sun'

Citation: Appl. Phys. Lett. **109**, 023110 (2016); doi: 10.1063/1.4959083
View online: http://dx.doi.org/10.1063/1.4959083
View Table of Contents: http://aip.scitation.org/toc/apl/109/2
Published by the American Institute of Physics

Articles you may be interested in

Giant negative thermal expansion covering room temperature in nanocrystalline GaNxMn3
Appl. Phys. Lett. **107**, 131902131902 (2015); 10.1063/1.4932067

Colossal negative thermal expansion with an extended temperature interval covering room temperature in fine-powdered Mn0.98CoGe
Appl. Phys. Lett. **109**, 241903241903 (2016); 10.1063/1.4972234

Tunable negative thermal expansion related with the gradual evolution of antiferromagnetic ordering in antiperovskite manganese nitrides Ag1-xNMn3+x ($0 \le x \le 0.6$)
Appl. Phys. Lett. **106**, 082405082405 (2015); 10.1063/1.4913663

Magnetically driven negative thermal expansion in antiperovskite Ga1-xMnxN0.8Mn3 ($0.1 \le x \le 0.3$)
Appl. Phys. Lett. **107**, 202406202406 (2015); 10.1063/1.4936239

Tunable thermal expansion and magnetism in Zr-doped ScF3
Appl. Phys. Lett. **109**, 181901181901 (2016); 10.1063/1.4966958

Giant isotropic magnetostrain of GaCMn3
Appl. Phys. Lett. **110**, 062405062405 (2017); 10.1063/1.4975980

Size effects on negative thermal expansion in cubic ScF_3

C. Yang,[1,2] P. Tong,[1,a)] J. C. Lin,[1] X. G. Guo,[1,2] K. Zhang,[1,2] M. Wang,[1] Y. Wu,[1] S. Lin,[1] P. C. Huang,[2,3] W. Xu,[1] W. H. Song,[1] and Y. P. Sun[1,3,4,b)]
[1]*Key Laboratory of Materials Physics, Institute of Solid State Physics, Chinese Academy of Sciences, Hefei 230031, China*
[2]*University of Science and Technology of China, Hefei 230026, China*
[3]*High Magnetic Field Laboratory, Chinese Academy of Sciences, Hefei 230031, China*
[4]*Collaborative Innovation Center of Advanced Microstructures, Nanjing University, Nanjing 210093, China*

(Received 13 April 2016; accepted 6 July 2016; published online 15 July 2016)

Scandium trifluoride (ScF_3), adopting a cubic ReO_3-type structure at ambient pressure, undergoes a pronounced negative thermal expansion (NTE) over a wide range of temperatures (10 K–1100 K). Here, we report the size effects on the NTE properties of ScF_3. The magnitude of NTE is reduced with diminishing the crystal size. As revealed by the specific heat measurement, the low-energy phonon vibrations which account for the NTE behavior are stiffened as the crystal size decreases. With decreasing the crystal size, the peaks in high-energy X-ray pair distribution function (PDF) become broad, which cannot be illuminated by local symmetry breaking. Instead, the broadened PDF peaks are strongly indicative of enhanced atomic displacements which are suggested to be responsible for the stiffening of NTE-related lattice vibrations. The present study suggests that the NTE properties of ReO_3-type and other open-framework materials can be effectively adjusted by controlling the crystal size. *Published by AIP Publishing.* [http://dx.doi.org/10.1063/1.4959083]

Most materials expand when heated; so exceptions always attract much attention because of rich underlying physics and great potential applications. The emergence of negative thermal expansion (NTE) in materials brings us opportunities of designing materials with special thermal properties, such as zero thermal expansion (ZTE), which are valuable in many fields.[1–14] Over the past years, several mechanisms have already been proposed to explain this interesting property, such as magnetic transition in Invar alloys[1] and Mn-based antiperovskite compounds,[2–8] spontaneous polarization in $PbTiO_3$-based ferroelectrics,[9] and change of electronic configuration in $LaCu_3Fe_4O_{12}$ and $BiNiO_3$.[10,11]

Beyond those, NTE in open-framework materials, like ZrW_2O_8,[12] always involves phonon-related transverse cooperative vibrations. The related phonon modes are originated from the coupled rocking of rigid coordination polyhedral units in these materials.[12,13] However, in most cases, the crystal structures are so complex that the NTE mechanism is hard to be displayed clearly.[15,16] Therefore, for further study of NTE in open-framework materials, the much simpler cubic ReO_3-type structure is often used to illustrate how rigid unit vibrational modes (RUMs) and the associated transverse thermal motion of bridging atoms can lead to volumetric contraction on heating.[17,18] Scandium trifluoride (ScF_3), a typical ReO_3-type NTE compound, remains cubic from at least 10 K to 1600 K at ambient pressure and has an isotropic NTE with the linear coefficient of thermal expansion (CTE), $\alpha_L \sim -14$ ppm/K between 60 K and 110 K.[14] Over the past years, researchers have made a great effort to control its CTE by chemical doping and already made significant achievements.[19–22] Morelock *et al.* reported their systematical study of CTE controlling in ScF_3 via solid solution formation with AlF_3, TiF_3, and YF_3.[19–21] A phase transition from cubic to rhombohedral was induced in the solid solutions and the transition temperature increases with the addition of doping content.[19–21] In the rhombohedral phase, $Sc_{1-x}M_xF_3$ (M = Al, Ti, and Y) exhibits positive thermal expansion (PTE) in contrast with NTE in the cubic phase so that the CTE could be effectively tuned by adjusting the dopant's concentration. Hu *et al.* obtained ZTE over a wide temperature range (300 K–900 K) in $(Sc_{0.85}Ga_{0.05}Fe_{0.1})F_3$.[22] Although the average structure is cubic, it is locally distorted to be rhombohedral. Such a local structure distortion was proposed to be responsible for the ZTE obtained in $(Sc_{0.85}Ga_{0.05}Fe_{0.1})F_3$.[22] Recent theoretical works proposed that the weakened NTE of $(Sc_{1-x}M_x)F_3$ can be attributed to the size mismatch between Sc^{3+} and other doping M^{3+} ions.[23,24] This mismatch has an effect on the lattice similar to the pressure effect, to which the structure of ScF_3 is extremely sensitive.[14,23,24]

In addition to chemical substitution, the crystal size can also affect the CTE in NTE materials.[5,6,8,9] The strong NTE of $PbTiO_3$-$BiFeO_3$ ferroelectrics is initially weakened and then transformed to PTE as the crystal size is gradually reduced, which is highly associated with the weakening of ferroelectricity.[9] The temperature region of lattice contraction was found to be extended in nanocrystalline $Cu_{1-x}Ge_xNMn_3$[5,8] and GaN_xMn_3[6] in comparison with bulk samples. In open-framework ZrW_2O_8, the reported size effects on NTE are quite controversial. Sun *et al.* reported that when the crystal size of ZrW_2O_8 is decreased to nanometer range, the NTE was in a diminished trend.[25] However, Wu *et al.* documented that the magnitude of the NTE coefficient in nanosized ZrW_2O_8 crystals is about 30% larger than that of the bulk sample.[26] Here, we report the size effects on NTE in simple cubic ScF_3. As the average crystal size is reduced

a)E-mail: tongpeng@issp.ac.cn
b)E-mail: ypsun@issp.ac.cn

from micron to nano scale, the NTE is gradually weakened. Moreover, the peak in the specific heat C_pT^{-3}-T plot, which is closely related to the transverse thermal vibrations,[27–30] is shifted to higher temperatures as the crystal size reduces. The stiffened transverse thermal vibrations and the reduced NTE magnitude can be attributed to the enhanced statically atomic displacements in nano-sized ScF_3 as revealed by high-energy X-ray pair distribution function (PDF). Moreover, the cubic crystal symmetry is maintained both macroscopically and locally as the crystal size is reduced.

The minor ScF_3 cubes were made from $Sc(NO_3)_3$ (3 N, Alfa Aesar) and NH_4F (Alfa Aesar) by solvothermal synthesis similar to previous works.[31] For a typical procedure, 0.001 mol $Sc(NO_3)_3$ and 0.006 mol NH_4F (the excess fluorine ions to improve productivity) were dissolved in a mixture of 25 ml deionized water and 5 ml ethylene glycol in a 50 ml Teflon-lined stainless autoclave, which was sealed and maintained at 150 °C–200 °C for 1 h–100 h, in order to obtain different-sized ScF_3. After the autoclave was cooled to room temperature, the resulting precipitates were washed by deionized water and anhydrous ethanol for more than 3 times, respectively, and separated by centrifugation. The white powders collected were dried at 60 °C for 5 h.

Crystal structures and lattice parameters were characterized by X-ray diffraction (XRD) using a Philips X'pert PRO X-ray diffractometer with Cu K_α radiations ($K_{\alpha1} = 1.5406$ Å, $K_{\alpha2} = 1.5418$Å) under ambient conditions. On the same X-ray diffractometer, temperature dependent XRD experiments were conducted to determine the CTE of each sample. PDFs were obtained from the high-energy X-ray scattering carried out on an in-house X-ray diffractometer (Bruker D8 Discover) equipped with an X-ray tube of the Ag anode (=0.56 Å).[7] The specific heat capacities were measured by a Physical Property Measurement System (Quantum Design). To minimize experimental error and ensure accuracy of heat capacity data of different samples, each sample was made into a small square pellet with nearly the same mass (0.006 g). Scanning electron microscopy (SEM) images were taken on a scanning electron microscope (FE-SEM, FEI-designed Sirion 200, FEI, Hillsboro, OR) operated at 5 kV. The infrared and Raman spectra were measured on a NEXUS infrared spectrometer (Thermo Nicolet) and a Horiba Jobinyvon T64000 Raman Spectrometer, respectively. Thermogravimetric data were collected on a Thermogravimetric Analyzer (Perkin-Elmer Pyris 1 TGA).

A small amount of $(NH_4)_3ScF_6$ impurity is always presented in the products if solvothermal reaction temperature is below 150 °C. When the reaction temperature ranges from 150 °C to 200 °C, it has little effect on the average crystal size of ScF_3 cubes, while the crystal size of ScF_3 depends remarkably on the reaction time. We note that in this method, when the reaction time is less than 2 h, the above impurity will also appear (Fig. S1 in supplementary material).[32] On the other hand, the size will no longer increase if the reaction time is longer than 100 h. So the ScF_3 samples prepared at 200 °C with a reaction time of 2 h, 10 h, and 100 h were used for further measurements. The morphology and crystal size of all the three samples were measured by a FE-SEM as shown in Fig. 1, where isotropic ScF_3 cubic crystals are clearly seen. The average crystal sizes were

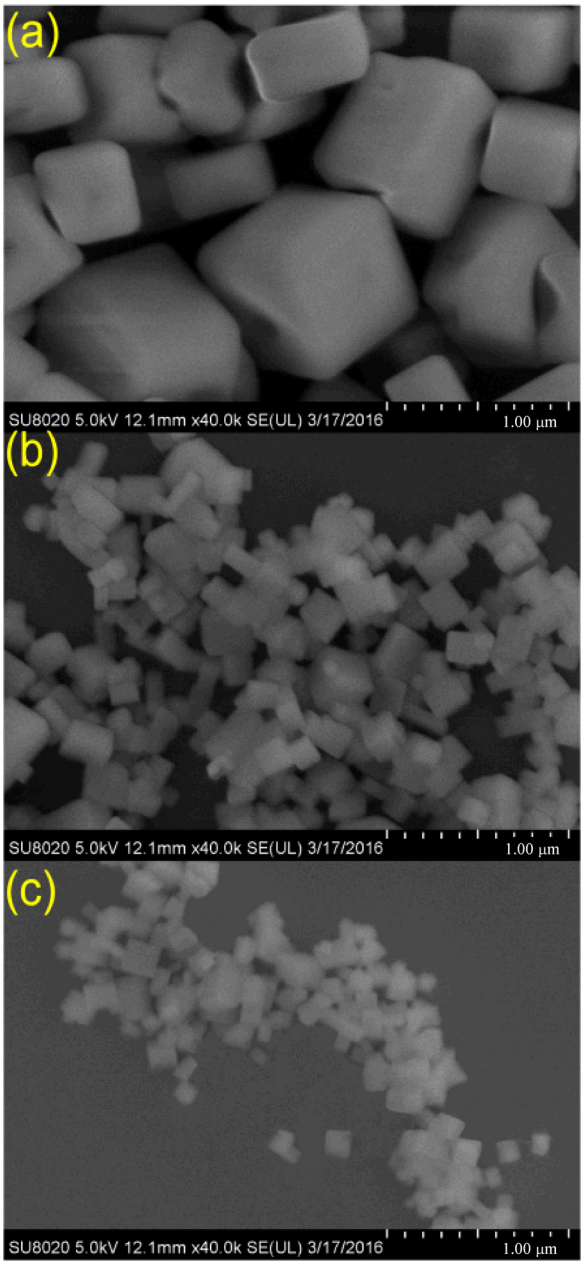

FIG. 1. FE-SEM images of ScF_3 samples with average sizes of 1 μm (a), 0.3 μm (b), and 80 nm (c).

estimated to be 80 nm, 0.3 μm, and 1 μm for the 2-h, 10-h, and 100-h prepared samples, respectively. The results of TGA, Raman, and infrared spectra indicate that hydroxides are absent or too little to be detected in our samples (Figs. S2–S4 in supplementary material).[32]

Fig. 2(a) shows the XRD patterns of ScF_3 samples with different sizes, suggesting that all the samples adopt the cubic ReO_3-type structure (space group, $Pm\text{-}3m$). With minimizing the crystal size, the diffraction peaks become wider and peak positions slightly shift to higher angles, as shown by the (200) peaks in Fig. 2(b). The size-dependent lattice constants at room temperature were obtained from standard Rietveld refinement (Fig. S5 in supplementary material).[32] As plotted in the insert image of Fig. 2(a), the overall lattice tends to shrink gradually with the decreasing crystal size. This is fairly normal for nanocrystalline materials because

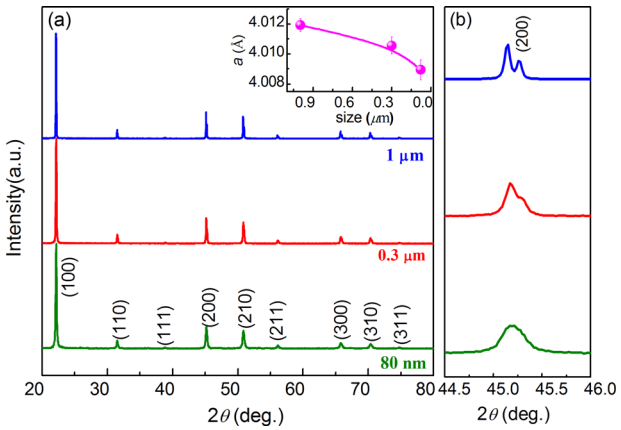

FIG. 2. (a) XRD patterns and (b) (200) diffraction peak of different-sized ScF_3 samples at room temperature. The inset of (a) shows the size-dependence of lattice constant, *a*.

the interface/grain boundary stress adds a hydrostatic pressure on the lattice and leads to a volume contraction.[33]

Linear thermal expansion $\Delta a/a$(113 K) based on temperature dependent XRD data from 113 K to 613 K (Fig. S6 in supplementary material)[32] is presented in Fig. 3 for different-sized ScF_3 samples. It can be seen that as crystal size decreases, the NTE of ScF_3 was gradually weakened. To give a more clear insight, the linear fitting of thermal expansion $\Delta a/a$(313 K) from 113 K to 313 K is displayed in the inset of Fig. 3. The obtained CTE is −9.49 ppm/K, −8.35 ppm/K, and −6.92 ppm/K, corresponding to the 1-μm, 0.3-μm, and 80-nm samples, respectively. The average CTE above room temperature (313 K–593 K) is also remarkably changed from −4.82 ppm/K for the 1-μm sample to −2.51 ppm/K for the 80-nm sample.

In many open-framework thermomiotic materials, such as ZrW_2O_8, $Y_2Mo_3O_{12}$, and $Sc_2M_3O_{12}$ (M = W and Mo),[28–30] the NTE is highly correlated with the low-dispersion low-frequency phonon modes. Those low-energy modes usually give rise to an excess contribution to the low-temperature specific heat beyond the Debye contribution (the well-known T^3 law).[28] Similarly, a large low-temperature peak was observed in the C_pT^{-3}-T curve for ScF_3 and attributed to NTE-associated low-energy phonon modes.[27] Heat capacity studies of different-sized ScF_3 are presented in Fig. 4. In the C_pT^{-3}-T curve of 1-μm ScF_3, a low-temperature peak exceeding Debye contribution is clearly seen. The peak height value is about 0.43 mJ $K^{-4}mol^{-1}$, which is very similar in magnitude to those of other thermomiotic materials (0.3 mJ $K^{-4}mol^{-1}$ for ZrW_2O_8,[28] 0.4 mJ $K^{-4}mol^{-1}$ for $Y_2Mo_3O_{12}$,[29] and 0.2 mJ $K^{-4}mol^{-1}$ for $Sc_2W_3O_{12}$[30]). The peak value in the C_pT^{-3}-T curve decreases to 0.35 mJ $K^{-4}mol^{-1}$ and 0.25 mJ $K^{-4}mol^{-1}$ for 0.3-μm and 80-nm ScF_3 samples, respectively. Moreover, the peak position shifts to higher temperatures as the crystal size decreases. The weakened and blue-shifted peak in the C_pT^{-3}-T curve clearly suggests a suppression of the NTE-related low-energy thermal vibrations, which accounts for the reduction of NTE magnitude as shown in Fig. 3. It is notable that the peak values of the C_pT^{-3}-T curve are lower than the previously reported value of ScF_3 powders (about 0.54 mJ $K^{-4}mol^{-1}$) made by solid state reaction.[27] It in turn explains why the NTE coefficient (−9.49 ppm/K, 113 K–273 K) in our 1-μm ScF_3 sample is a little smaller in magnitude than the previously reported one (−10 ppm/K, 115 K–274 K).[14]

In chemically doped $Sc_{1-x}M_xF_3$, either overall or local structure instability was proposed to be responsible for the suppression of NTE.[19–22] Our temperature dependent XRD patterns did not give any hints of symmetry change in the whole temperature range investigated (Figs. 2, S5 and S6 in supplementary material[32]). In order to check the possible local structure distortion, high energy X-ray scattering was carried out for 80-nm and 1-μm samples on an X-ray diffractometer equipped with Ag anode.[7] Collected data were subjected to routine corrections and background subtraction, and finally the atomic PDF, G(r)s (Fig. 5(a)), was obtained via a Fourier transformation.[34] We tested the G(r)s using the average cubic model (space group, *Pm-3m*) as well as the rhombohedral model (space group, *R-3c*). For both samples, the G(r) data can be reasonably described by the cubic model, though the *R-3c* model gives rise to a better fitting to the data for both samples (Fig. S7 in supplementary material).[32] This is not surprising because, in the *R-3c* model, four more

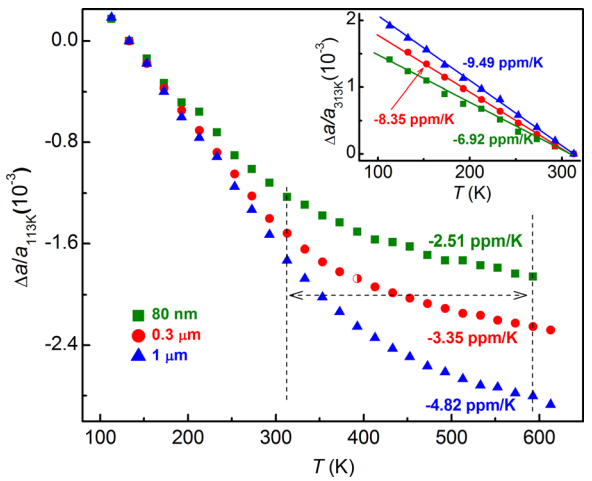

FIG. 3. Thermal expansion $\Delta a/a$(113 K) calculated from temperature dependent XRD between 113 K and 613 K for different-sized ScF_3 samples. The inset shows a linear fitting of thermal expansion $\Delta a/a$(313 K) from 113 K to 313 K for all samples. The average (313 K–593 K) and linear (113 K–313 K) CTEs are shown for all samples in the main panel and inset, respectively.

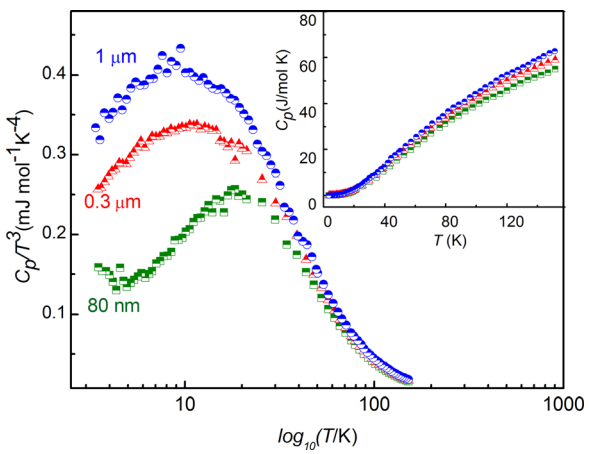

FIG. 4. The experimental molar heat capacity of different-sized ScF_3 samples expressed as C_pT^{-3}-T. The inset presents the original temperature-dependent heat capacity for the three samples.

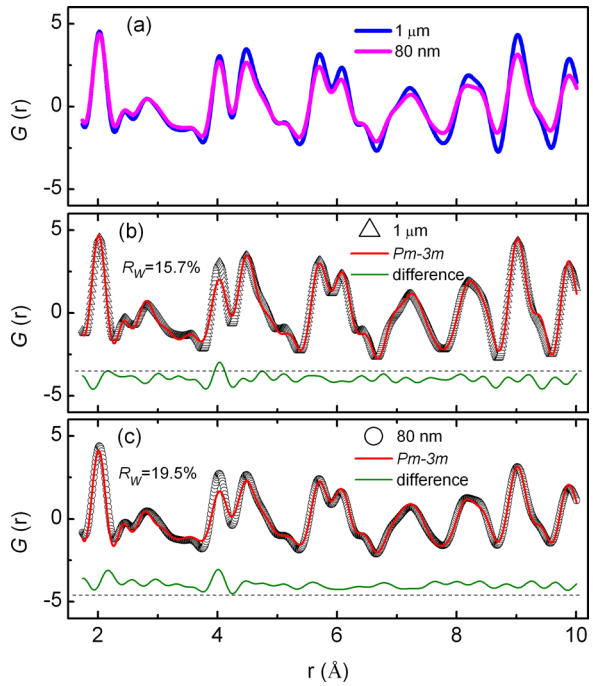

FIG. 5. Pair distribution function, G(r), obtained from high energy X-ray total scattering data collected at room temperature. (a) shows a comparison of G(r)s for 1-μm and 80-nm ScF_3 samples. Calculated G(r) using the *Pm-3m* model (the red line) together with the experimental G(r) (circle) for 1-μm (b) and 80-nm (c) ScF_3 samples. The difference between calculated G(r) and experimental G(r) is shown at the bottom in each panel. The agreement factor of fitting, R_w, was listed in (b) and (c).

parameters are allowed to change compared with those in the cubic model (Table SI in supplementary material).[32] Relative to the cubic model, the *R-3c* model leads to a reduction in the agreement factor (R_w) by 22.3% for the 1-μm sample. While for the case of the 80-nm sample, a smaller reduction of R_w (16.4%) was observed. Clearly, for the 80-nm sample, the *R-3c* model did not give a particular improvement for the fitting of G(r). In other words, the local structure of 80-nm sample is lacking rhombohedral distortion. The lattice constant resulting from G(r) profile fitting also decreases as the crystal size is reduced (Table SI in supplementary material),[32] in agreement with the result based on the average lattice constant (inset of Fig. 2(a)).

Moreover, compared with the 1-μm sample, the 80-nm sample's G(r) peaks become wider with smaller intensity, which accumulates with distance, r. Such modifications of G(r) peaks have been widely observed in nanocrystalline materials (e.g., ZnS,[35] $BiFeO_3$,[36] and GaN_xMn_3[6]) and been attributed to the static displacements of atoms beyond thermal vibrations. The enhanced static disorders and reduced structural coherence are beyond the protocol of crystal symmetry, which may explain why the G(r)'s fitting for the 80-nm sample is always worse than that for the 1-μm sample whatever model is used.

The phonon frequency's blue shift has often been observed in nano-sized semiconductors.[37,38] Although a unified comprehension is not yet reached, it is widely accepted that such a behavior is closely related to the small-size effects (e.g., surface pressure and phonon confinement effect).[37,38] As the crystal size is reduced from 1 μm to 80 nm, the resulting surface pressure calculated from the volume contraction (~0.22%) is about 0.1198 GPa, according to the previously reported pressure-lattice relation of ScF_3.[14] It has been confirmed that the CTE of ScF_3 between 298 K and 523 K is not affected under hydrostatic pressure up to 0.3 GPa (above which the data are not available).[39] In contrast, the high-temperature NTE is significantly weakened in our case as displayed in Fig. 3. Therefore, the surface pressure effect contributes little to the change of NTE. Only when the crystal size is smaller than 10 nm, should the phonon confinement be taken into account in studying the phonon vibrations.[37,38] Thus, the phonon confinement mechanism is not applicable here due to the relatively large crystal size of our samples (≥80 nm). As demonstrated in nanosized ZnS, the lattice stiffening can be attributed to the atomic disorders, i.e., the atoms statically deviate from their ideal positions.[35] As revealed by PDF analysis, the nanocrystals are characteristic of a large distribution of bond lengths.[6,35] All deviations from the equilibrium bond lengths were suggested to increase the vibration frequency.[35] Moreover, the C_pT^{-3}-T curve of non-NTE ReO_3 does not show any peak features, which was attributed to the enhanced static disorders proved by neutron diffractions.[40] Consequently, the stiffening of NTE-related phonon modes can be attributed to the static atomic disorders as manifested by the broadening of PDF peaks (Fig. 5).

In summary, ScF_3 samples with different crystal sizes are fabricated by the solvothermal method. With the crystal size going smaller, weakened NTE was observed. This can be attributed to the stiffening of low-energy phonon modes as manifested by the blue shift of the C_pT^{-3}-T peak. PDF analysis excludes the symmetry breaking as the origin of weakened NTE, which was previously proposed for the cases of chemically doped ScF_3. Instead, enhanced atomic displacements beyond the thermal vibrations were observed, which are suggested to be responsible for the stiffening of the lattice vibrations and consequently for the weakened NTE magnitude. The current study demonstrated that the NTE of ScF_3 can be effectively controlled by manipulating the crystal size, which might also be applicable to other open-framework materials.

This work was supported by the National Key Basic Research under Contract No. 2011CBA00111, the National Natural Science Foundation of China under Contract Nos. 51322105, 11174295, 51301167, 51171177, 91222109 and 51301162 and the Hefei Science Center CAS (2015HSC-UP002). C. Y. thanks Dr. Chen Sun from University of Wisconsin-Madison for her assistance in editing the revised manuscript.

[1]P. Mohn, Nature **400**, 18 (1999).
[2]K. Takenaka and H. Takagi, Appl. Phys. Lett. **87**, 261902 (2005).
[3]K. Takenaka and H. Takagi, Appl. Phys. Lett. **94**, 131904 (2009).
[4]Y. Sun, C. Wang, Y. C. Wen, K. G. Zhu, and J. T. Zhao, Appl. Phys. Lett. **91**, 231913 (2007).
[5]X. Y. Song, Z. H. Sun, Q. Z. Huang, M. Rettenmayr, X. M. Liu, M. Seyring, G. N. Li, G. H. Rao, and F. X. Yin, Adv. Mater. **23**, 4690 (2011).
[6]J. C. Lin, P. Tong, X. J. Zhou, H. Lin, Y. W. Ding, L. Chen, X. G. Guo, C. Yang, B. Song, Y. Wu, S. Lin, W. H. Song, and Y. P. Sun, Appl. Phys. Lett. **107**, 131902 (2015).
[7]X. G. Guo, J. C. Lin, P. Tong, M. Wang, Y. Wu, C. Yang, B. Song, S. Lin, W. H. Song, and Y. P. Sun, Appl. Phys. Lett. **107**, 202406 (2015).

[8]J. Tan, R. J. Huang, W. Wang, W. Li, Y. Q. Zhao, S. P. Li, Y. M. Han, C. J. Huang, and L. F. Li, Nano Res. **8**, 2302 (2015).
[9]J. Chen, L. L. Fan, Y. Ren, Z. Pan, J. X. Deng, R. B. Yu, and X. R. Xing, Phys. Rev. Lett. **110**, 115901 (2013).
[10]M. Azuma, W. T. Chen, H. Seki, M. Czapski, K. Oka, M. Mizumaki, T. Watanuki, N. Ishimatsu, N. Kawamura, and S. Ishiwata, Nat. Commun. **2**, 347 (2011).
[11]Y. Long, N. Hayashi, T. Saito, M. Azuma, S. Muranaka, and Y. Shimakawa, Nature **458**, 60 (2009).
[12]T. A. Mary, J. S. O. Evans, T. Vogt, and A. W. Sleight, Science **272**, 90 (1996).
[13]A. L. Goodwin, M. Calleja, M. J. Conterio, M. T. Dove, J. S. Evans, D. A. Keen, L. Peters, and M. G. Tucker, Science **319**, 794 (2008).
[14]B. K. Greve, K. L. Martin, P. L. Lee, P. J. Chupas, K. W. Chapman, and A. P. Wilkinson, J. Am. Chem. Soc. **132**, 15496 (2010).
[15]M. G. Tucker, A. L. Goodwin, M. T. Dove, D. A. Keen, S. A. Wells, and J. S. O. Evans, Phys. Rev. Lett. **95**, 255501 (2005).
[16]K. W. Chapman, P. J. Chupas, and C. J. Kepert, J. Am. Chem. Soc. **127**, 15630 (2005).
[17]P. B. Allen, Y. R. Chen, S. Chaudhuri, and C. P. Grey, Phys. Rev. B **73**, 172102 (2006).
[18]Y. M. Liu, Z. H. Wang, M. Y. Wu, Q. Sun, M. J. Chao, and Y. Jia, Comput. Mater. Sci. **107**, 157 (2015).
[19]C. R. Morelock, B. K. Greve, L. C. Gallington, K. W. Chapman, and A. P. Wilkinson, J. Appl. Phys. **114**, 213501 (2013).
[20]C. R. Morelock, L. C. Gallington, and A. P. Wilkinson, Chem. Mater. **26**, 1936 (2014).
[21]C. R. Morelock, L. C. Gallington, and A. P. Wilkinson, J. Solid State Chem. **222**, 96 (2015).
[22]L. Hu, J. Chen, L. L. Fan, Y. Ren, Y. C. Rong, Z. Pan, J. X. Deng, R. B. Yu, and X. R. Xing, J. Am. Chem. Soc. **136**, 13566 (2014).
[23]S. U. Handunkanda, E. B. Curry, V. Voronov, A. H. Said, G. G. Guzman-Verri, R. T. Brierley, P. B. Littlewood, and J. N. Hancock, Phys. Rev. B **92**, 134101 (2015).
[24]P. Lazar, T. Bucko, and J. Hafner, Phys. Rev. B **92**, 224302 (2015).
[25]X. J. Sun, J. Yang, Q. Q. Liu, and X. N. Cheng, J. Alloys Compd. **481**, 668 (2009).
[26]H. C. Wu, P. Badrinarayanan, and M. R. Kessler, J. Am. Ceram. Soc. **95**, 3643 (2012).
[27]C. P. Romao, C. R. Morelock, M. B. Johnson, J. W. Zwanziger, A. P. Wilkinson, and M. A. White, J. Mater. Sci. **50**, 3409 (2015).
[28]A. P. Ramirez and G. R. Kowach, Phys. Rev. Lett. **80**, 4903 (1998).
[29]C. P. Romao, K. J. Miller, M. B. Johnson, J. W. Zwanziger, B. A. Marinkovic, and M. A. White, Phys. Rev. B **90**, 024305 (2014).
[30]Y. Yamamura, S. Ikeuchi, and K. Saito, Chem. Mater. **21**, 3008 (2009).
[31]L. Hu, J. Chen, Z. Pan, J. X. Deng, R. B. Yu, and X. R. Xing, J. Am. Ceram. Soc. **97**, 1386 (2014).
[32]See supplementary material at http://dx.doi.org/10.1063/1.4959083 for XRD patterns and Rietvelt refinements for all samples, TGA, Raman and infrared spectra for 80-nm sample, and PDF fitting of *R-3C* model and related fitting parameters.
[33]G. K. Rane, U. Welzel, S. R. Meka, and E. J. Mittemeijer, Acta Mater. **61**, 4524 (2013).
[34]P. Tong, D. Louca, G. King, A. Llobet, J. C. Lin, and Y. P. Sun, Appl. Phys. Lett. **102**, 041908 (2013).
[35]B. Gilbert, F. Huang, H. Z. Zhang, G. A. Waychunas, and J. F. Banfield, Science **305**, 651 (2004).
[36]V. Petkov, S. M. Selbach, M. A. Einarsrud, T. Grande, and S. D. Shastri, Phys. Rev. Lett. **105**, 185501 (2010).
[37]L. H. Liang, C. M. Shen, X. P. Chen, W. M. Liu, and H. J. Gao, J. Phys.: Condens. Matter **16**, 267 (2004).
[38]C. Q. Sun, L. K. Pan, C. M. Li, and S. Li, Phys. Rev. B **72**, 134301 (2005).
[39]C. R. Morelock, "Thermal expansion, compressibility, and local structure of fluorides and oxyfluorides with the rhenium trioxides structure," Ph.D. thesis, Georgia Institute of Technology (2014).
[40]E. E. Rodriguez, A. Llobet, T. Proffen, B. C. Melot, R. Seshadri, P. B. Littlewood, and A. K. Cheetham, J. Appl. Phys. **105**, 114901 (2009).